LBL-19939

Lawrence Berkeley Laboratory
UNIVERSITY OF CALIFORNIA

Accelerator & Fusion
Research Division

Presented at the Seventh International Free
Electron Laser, Tahoe, CA, September 8-13, 1985

A STEADY-STATE FEL: PARTICLE DYNAMICS IN THE FEL PORTION OF A TWO-BEAM ACCELERATOR

E. Sternbach and A.M. Sessler

September 1985

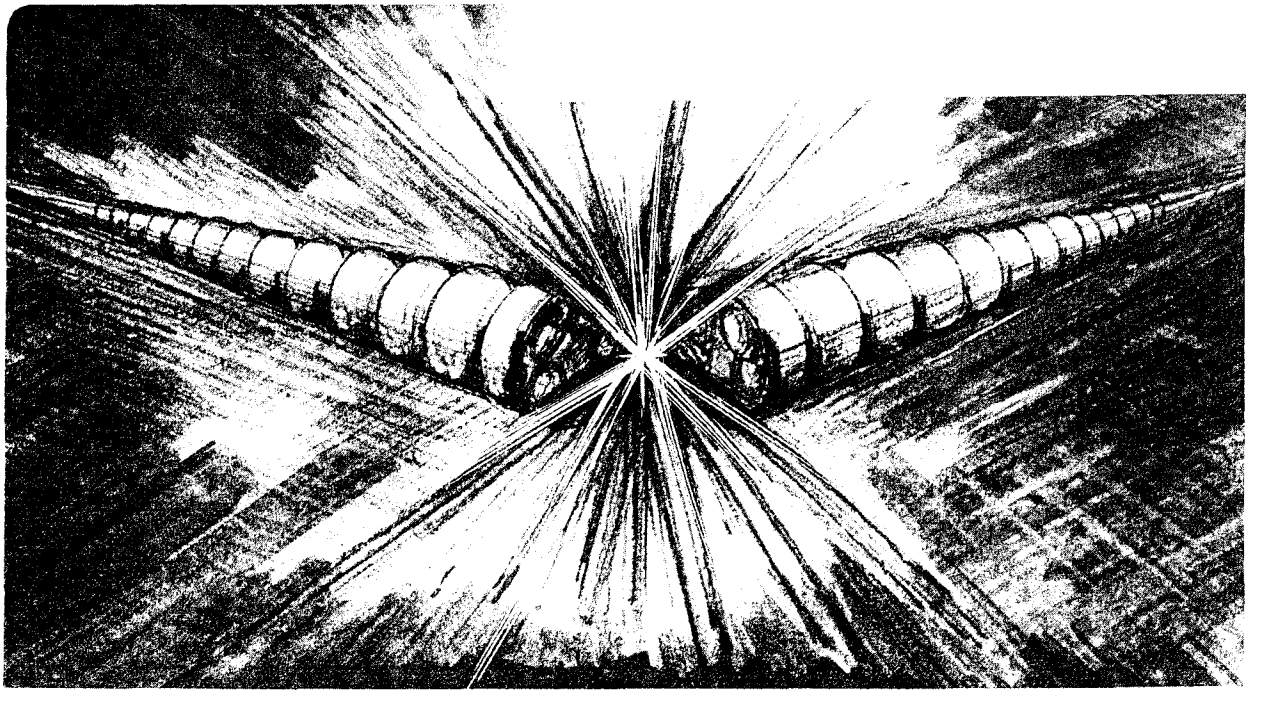

Prepared for the U.S. Department of Energy under Contract DE-AC03-76SF00098

A STEADY-STATE FEL: PARTICLE DYNAMICS IN THE FEL PORTION OF A TWO-BEAM ACCELERATOR*

Efrem Sternbach and Andrew M. Sessler

Lawrence Berkeley Laboratory
University of California
Berkeley, CA 94720

ABSTRACT

Motivated by its use in a Two-Beam Accelerator, we have studied a "steady-state" FEL; i.e., a periodic but very long structure in which the electron beam energy is replenished once a period with a short induction acceleration unit. We have studied longitudinal particle motion in such a device using a 1-D simulation code. We show that after an initial start-up section, particle detrapping from the pondermotive wave is minimal in a steady-state FEL of several kilometers. A simple linear model of particle diffusion is shown to describe the numerical results quite well.

---

* This work was supported by the Division of High Energy Physics, U.S. Department of Energy, under Contract No. DE-AC03-76SF00098.

I. Introduction

With the imminent completion of, and expected successful operation of, the Stanford Linear Collider (SLC), accelerator physicists are planning the next generation of linear colliders. These would seem to require a higher accelerating gradient and a reasonably efficient use of power. One possibility is to operate the accelerator power source at a significantly higher frequency than the SLC (2.8 GHz), perhaps in the 30 GHz range. At the present time no suitable power source exists at this frequency (although considerable effort is being devoted to developing high-power sources at frequencies above 2.8 GHz). It has been proposed that a "steady-state" FEL could be used to power the accelerator,[1] in a suggested configuration called a Two-Beam Accelerator (TBA).

A schematic of a TBA is shown in Fig. 1. In this scheme a low energy, high current electron beam is fed into a tapered wiggler module. The generated microwave power is piped out of the FEL waveguide and is used to power the high gradient accelerating structure. At the end of each wiggler module, an induction unit is used to replace the electron beam energy that was lost in the wiggler. This ideal steady-state FEL, it will be shown, could be as long as is needed (limited in a practical design by considerations of "filling time" of the high gradient structure and "slippage" between the high energy bunch and the low-energy FEL beam). In this paper we examine longitudinal effects in the FEL beam.

II. Design of Steady State FEL

A TBA has been simulated using the 1-D FEL equations of motion in a rectangular waveguide. All subsequent equations are for a system where the

beam radius is assumed small compared with the waveguide dimensions. The 1-D FEL equations for a TE mode are:[2]

$$\frac{d\gamma_j}{dz} = \frac{-\omega}{c} a_s a_w \frac{\sin \psi_j}{\gamma_j} \quad , \tag{1a}$$

$$\frac{d\psi_j}{dz} = (k_w - \delta k_s) - \frac{\omega}{2c\gamma_j^2}(1 + a_w^2 - 2a_w a_s \cos \psi_j) + \frac{d\phi}{dz} \quad , \tag{1b}$$

$$\frac{da_s}{dz} = \frac{\omega_{p,eff}^2 a_w}{2\omega c} \left\langle \frac{\sin \psi}{\gamma} \right\rangle - \alpha a_s \quad , \tag{1c}$$

$$\frac{d\phi}{dz} = \frac{\omega_{p,eff}^2 a_w}{2\omega c a_s} \left\langle \frac{\cos\psi}{\gamma} \right\rangle \quad ,$$

where j is an index denoting a particular particle and <> indicates an average over particles. These equations are an extension of the KMR equations[3] for an FEL. In these equations, the dispersion relation for a waveguide relates ω and k_s. The factor δk_s results because the phase velocity of radiation in a waveguide is not equal to c. Specifically for a $TE_{\ell n}$ mode:

$$k_s = \left[\left(\frac{\omega^2}{c^2} - \left(\frac{2\pi\ell}{a}\right)^2 - \left(\frac{2\pi n}{b}\right)^2\right]^{1/2} \quad , \tag{2a}$$

$$\delta k_s = \frac{\omega}{c} - k_s \quad , \tag{2b}$$

where a and b are respectively the x and y dimensions of the waveguide. It is also important to note that the plasma frequency in equations (1c) and (1d) is an effective plasma frequency given by

$$\omega_{p,eff}^2 = \frac{8\pi e I}{mcab} \quad , \tag{3}$$

where I is the total beam current and m and e are respectively the electron mass and charge. The factor α in Eq. (1c) is a loss factor meant to model the removal of microwave power from the FEL waveguide.

In designing a taper for an FEL it is useful to define the concept of a resonant particle. This is defined by setting $d\psi/dz = 0$. For an untapered wiggler this corresponds to a fixed point of the system in phase space. If the external parameters are varied adiabatically, one can think of this fixed point as being slowly changed in energy. One can define a resonant γ by:

$$\gamma_r^2 = \frac{\omega}{2c(k_w - \delta k_s + \frac{d\phi}{dz})} [1 + a_w^2 - 2a_w a_s \cos \psi_r] \quad . \tag{4}$$

This is more complicated than it looks since there is an additional γ_r dependence in the $d\phi/dz$ term. In the applications of this resonant particle concept we are interested in resonances for distributions of particles. If one assumes that the distribution will be symmetric around the resonance point, then one can approximate the a_s and ϕ equations as:

$$\frac{da_s}{dz} = \frac{\omega_{p,eff}^2 a_w k_s}{2 \omega^2 c} \frac{\sin \psi_r}{\gamma_r} - \alpha a_s \quad , \tag{5a}$$

$$\frac{d\phi}{dz} = \frac{\omega_{p,eff}^2 a_w k_s}{2 \omega^2 c} \frac{\langle \cos \psi \rangle}{\gamma_r} \quad . \tag{5b}$$

The factor $\langle \frac{\sin\psi}{\gamma} \rangle$ goes to $\frac{\sin\psi_r}{\gamma_r}$ since in real-world tapers, ψ_r is typically a very small number. Near $\psi=0$, $\sin\psi$ is an odd function and its average over the distribution is very nearly $\sin\psi_r$. For similar reasoning we must keep the $\cos\psi$ term as an average. The average of $\cos\psi$ over the distribution will be some number less than 1 • The factor $\langle\cos\psi\rangle$ is called the bunching parameter.

In a tapered wiggler, the magnetic field a_w is varied adiabatically with distance. The quantities γ_r, a_s and ϕ then evolve in a well defined manner. Over the course of the wiggler, an electron "sitting" on the resonance point would decrease in energy without changing its ψ coordinate at

all. During tapering one can also vary the factor α. This affects the evolution of the electric field a_s and therefore the resonant energy γ_r. In the designs in this report the factor α was varied so as to keep the quantity a_s a constant. A real TBA operating in a steady state would run at a nearly constant a_s.

III. TBA Simulation

A CRAY-XMP supercomputer was used to integrate the 1-D equations of motion. The tapered wigglers for the TBA were designed for a resonant particle. In the simulation a large number of particles were followed for the length of the FEL. The particles were bunched in an untapered wiggler before being injected into the TBA. The bunches were injected so that the particle distribution was centered as much as possible around the resonance point. The induction units at the end of each wiggler module were modeled as imparting an instantaneous jump in energy with no shift in phase. Table I shows the initial values used for the FEL design. Figure 2 shows the taper design used.

In a simulation where many particles are tracked according to the equations (1a)-(1d), the design process described works reasonably well. Equations (1c) and (1d) have averages that track the behavior of the particle distribution as a whole. What is seen in such a simulation is that at the beginning of the steady-state FEL, particles near the separatrix become detrapped rather quickly. However, particles near the resonance point remain trapped for long distances. If bunches are injected into the TBA such that the majority of the electrons are near the resonance point, then particle detrapping becomes negligible after a short distance. In Fig. 3 we show phase space plots of the electron distribution at different points in a wiggler module. The system at the distance shown is in a "steady-state."

Even with the 1-D apprpximation, the phase space trajectories of an electron in a steady-state FEL become quite complicated. An example is shown in Fig. 4. However, the dynamics of such a particle can be shown rather clearly if one makes a Poincaré plot of the particle trajectories. A Poincaré plot is made by taking a surface of section in phase space and plotting a point at each place a trajectory pierces the surface of section. This is reasonable since the steady-state FEL is a periodic system where every wiggler module and induction unit corresponds to a period. In Fig. 5 we show a Poincaré plot from a many-particle simulation. The plot is suggestive that the particle orbits move near surfaces that are tori in phase space. One might expect to be able to model the system in such a manner that the particle orbits lie on closed tori in phase space and some small perturbation causes diffusion between these tori.

IV. Motion in a Periodic Field

From Floquet theory, if the system of interest has a closed orbit, we can determine the stability of nearby orbits with respect to the closed orbit. This is equivalent to determining the stability of the Poincaré map about its fixed point.[4] In the Poincaré map that we wish to examine, there is a fixed point which is given by the resonance particle at the surface of section. To examine the stability of the mapping, we need to linearize the equations of motion around the resonance point. Linearizing (1a) and (1b) in γ and ψ gives

$$\frac{d(\delta\gamma)}{dz} = -\left(\frac{\omega a_s a_w \cos\psi_r}{c\gamma_r}\right)(\delta\psi) + \text{small terms}, \tag{6a}$$

$$\frac{d(\delta\psi)}{dz} = \frac{2(k_w + d\phi/dz - \delta k_s)}{\gamma_r}(\delta\gamma) + \text{small terms}. \tag{6b}$$

This system has eigenvalues that are purely imaginary. Thus one expects the

Poincaré mapping to be neutrally stable about the fixed point. This would correspond to center "orbits" with a frequency of

$$\omega_\ell = \left[\frac{2\,\omega\, a_s a_w\, k_w'\cos\psi_r}{c\gamma_r^2}\right]^{1/2} \quad , \tag{7}$$

where we have written $k_w' = k_w - \delta k_s + d\phi/dz$.

One can think of the Poincaré map as tracing out orbits around the resonance point. As we will show later, if a perturbation is superimposed on the electric field, it results in a set of linearized equations that look like a forced oscillator. If the forcing is not at the resonance frequency then the orbits will be shifted but their integrity will remain. If the forcing is at the resonance frequency (7), then the resonance point becomes unstable. This is illustrated in Fig. 6. In short, a purely periodic FEL can be designed so as to have no loss of particles.

V. Noise Theory

If one examines a plot of the electric field from an actual simulation (Fig. 7), it looks like there is noise superimposed on the intended value of the electric field. This "noise" in fact comes from the deterministic motion of the electrons around the resonance point. However, no detailed knowledge of particle orbits is necessary to describe the diffusion of particles across phase space.

Since the value of the resonance energy γ_r depends on the electric field a_s, then fluctuations in a_s should cause fluctuations in γ_r. We can then model the system as a harmonic oscillator whose equilibrium point is being shaken in some prescribed manner. To determine what the form of the forcing term should be, we can start with the Lagrangian

$$L = \frac{1}{2}\left[\frac{dx}{dz}\right]^2 - \frac{1}{2}\omega_\ell^2 \left[x - x_0(z)\right]^2 \quad , \tag{8}$$

where we use the notation $x = \delta\gamma$. The fluctuations are represented by $X_0(z)$ which describes the variation of γ from the design value of γ_r. The factor ω_ℓ also has a dependence on a_s, but in our system this causes a negligible effect on particle diffusion, so for simplicity it will be assumed to be constant.

It is convenient to introduce a dimensionless independent variable. We set $\tau = \omega_\ell z$. With this substitution Eq. (8) leads to an equation of motion

$$\frac{d^2x}{d\tau^2} + x = x_0(\tau) \tag{9}$$

This has a general solution

$$x(\tau) = A\cos\tau + B\sin\tau + \int_0^\tau d\tau'\, x_0(\tau')\sin(\tau-\tau') \tag{10}$$

Since we are interested in diffusion we many ignore the homogeneous terms which are needed to match initial conditions but don't give any x_0 related growth.

To calculate diffusion we wish to calculate $\langle x^2\rangle_\tau$ and retain the terms that go linearly with τ. In general

$$\langle x^2\rangle_\tau = \int_0^\tau d\tau' \int_{-\tau'}^{\tau-\tau'} ds\, \sin(\tau-\tau')\sin(\tau-\tau'-s)\, K(s) \tag{11}$$

and if $x_0(\tau)$ can be represented as noise[5], then $K(s) = \langle x_0(\tau)\, x_0(\tau+s)\rangle_\tau$ where $K(s)$ is called the correlation function for $x_0(\tau)$.

Now we must relate the correlation function for a_s with the correlation function for x_0. As the simplest approximation we expand γ_r in powers of a_s around the design value of a_{so}. The term linear in $a_s - a_{so}$ is then set equal to x_0. This gives, using equation (4):

$$x_0 = \kappa\,(a_s - a_{so}) = \kappa\,\delta a_s \quad ,$$

$$\text{where } \kappa = \left. \frac{\frac{d\phi}{dz} - \left[\frac{\omega}{c} \frac{a_s a_w \cos \psi_r}{\gamma_r^2}\right]}{2k_w' - \frac{d\phi}{dz}} \frac{\gamma_r}{a_s} \right| \text{ evaluated at } a_{so}. \tag{12}$$

Thus $\langle x_0(\tau)\ x_0(\tau + x)\rangle_\tau = \kappa^2 \langle \delta a_s(\tau)\ \delta a_s(\tau + s)\rangle\tau$

The correlation function for the electric field is shown in Fig. 8 for the parameters of Table I. Its Fourier transform is shown in Fig. 9.

If the frequency dependence is narrow, i.e., if the bandwidth is small with respect to the size of the average frequency, one can show that the diffusion goes like

$$\langle x^2 \rangle \cong \frac{\pi\kappa^2}{2} \tilde{f}\ (\Omega_0)\ \tau \quad , \tag{13}$$

$$= \frac{\pi\kappa^2}{2} \tilde{f}\ (\Omega_0)\ \omega_0 z \quad ,$$

where $f(\Omega_0)$ is the Fourier component of the noise in a_s at the oscillator frequency.

At this point it is important to note that both κ and ω_ℓ will change slowly over the course of a period. As a simple approximation, we will average the diffusion coefficient over a period. In Fig. 10 is shown the diffusion coefficient calculated from this theory. Table II shows some diffusion coefficients calculated from the computer simulation. Because of the great difficulty in measuring diffusion on the computer, these values do not exactly duplicate Fig. 10. It can be seen, however, that the order of magnitude is correct. In practice this should be quite sufficient since the Fourier spectrum of the electric field will vary some in different runs. Note that nonlinearities start to become important at about $\delta\gamma = 7$, which is about a third of the distance to the sepatrix. The linear analysis should be valid if most of the particles have orbits inside this. If one reviews Fig. 3 this

seems to be the case. In short, the diffusion of particles in a TBA is given by Equation (13), and by suitable design one can make this tolerably small.

VI. Induction Unit Fluctuations

In this section we look at an effect that is qualitatively different from that considered in the previous sections of this paper and yet can be explained by the same model. We ask what would happen if the induction units imparted a different energy than the wiggler tapers were designed for. We look at two cases. In the first case the induction units impart the wrong amount of energy to match onto the next tapered section but the mismatch is the same each time; i.e. we still have a periodic system. In the second case, there is no mismatch on the average, but the energy imparted to the particles fluctuates randomly with some maximum amplitude. In both cases we force γ_r to take the values calculated in the taper design.

To describe the effects of induction unit mismatch, we start by writing an expression for $x(\tau)$. Ignoring homogeneous terms gives

$$x(\tau) = \sum_{n}^{N} \Delta x(\omega_0 \ell n) \cos(\tau - \omega_0 \ell n)\, \theta(\tau - \omega_0 \ell n) \quad , \tag{14}$$

where ℓ is the distance between induction units, $\Delta x(\omega_0 \ell n)$ is the mismatch at the nth induction unit, N is the total number of induction units, and the step function θ indicates when each term "turns on." Equation (14) can be thought of as a sort of Green's function solution for a discrete system.

For the case where there is an identical mismatch in each section we can set $\Delta x(\omega_0 \ell n) = \Delta x_0$, a constant. To see if there is any diffusion we look at

$$x^2 = (\Delta x_0)^2 \sum_{n}^{N} \sum_{m}^{N} \cos(\tau - \omega_0 \ell n) \cos(\tau - \omega_0 \ell m)\, \theta(\tau - \omega_0 \ell n)\, \theta(\tau - \omega_0 \ell m) \tag{15}$$

If $\omega_0 \ell \neq 2\pi$, then x^2 is purely periodic and in fact should average to zero if N is large enough; i.e. there is no diffusion. Figure 11 shows a case run for a steady-state FEL where an induction unit that imparts $\Delta\gamma = 4$ is needed to match on, but the induction units actually used impart $\Delta\gamma = 5$. One might expect that such a large mismatch would certainly break up the invariant surfaces. As can be seen, the surfaces remain intact. This is actually a consequence of Floquet theory where as long as a perturbation is periodic and nonresonant, the qualitative properties of a system don't change. Even including non-linear terms, one should have invariant tori, up to some amplitude, as is well known in non-linear dynamics. If $\omega_0 \ell = 2\pi$, the system is at a resonance and becomes unstable.

If the induction unit mismatch is a random perturbation, then (14) becomes

$$\langle x^2 \rangle_\tau = \sum_n^N \sum_m^N \langle \Delta x^2 \rangle \, \delta_{m,n} \cos(\tau - \omega_0 \ell n) \cos(\tau - \omega_0 \ell n) \, \theta(\tau - \omega_0 \ell n) \, \theta(\tau - \omega_0 \ell n), \tag{16}$$

where the delta function is introduced due to the complete randomness of $\Delta x(\omega_0 \ell n)$. For a completely random function $\langle \Delta x^2 \rangle = \Delta x_{max}^2/3$. Thus we get

$$\langle x^2 \rangle_\tau = \frac{\Delta x_{max}^2}{3} \sum_n^N \cos^2(\tau - \omega_0 \ell n) \, \theta(\tau - \omega_0 \ell n) \tag{17}$$

If we now average over τ we get

$$\langle x^2 \rangle_\tau = \frac{\Delta x_{max}^2}{6} N \tag{18}$$

This equation describes the diffusion in phase space due to fluctuations in the induction units. In Fig. 12 we show a plot of diffusion coefficient verses oscillation amplitude. One can see in this plot that the nonlinearities start to become important around $\delta\gamma = x = 7$. This is a value

that is about 1/3 of the bucket height. Once more we expect the linear theory to be valid for the great majority of the particles.

VII. Transverse EFfects

We note that the equation governing small amplitude betatron motion is the Mathieu equation. The wave number of the oscillation is given by $k_\beta = k_w a_w/\sqrt{2}\gamma$. Ths system is unstable if the length of each module is equal to $n\pi/k_\beta$, where n is an integer. In practice these regions of instability should be narrow and easily avoided;[6] further work on transverse motion needs to be done, but the design of a TBA with stable transverse motion (in both planes) appears easily accomplished.

VIII. Conclusion

Within the 1-D FEL theory there seems to be no impediment to running a steady-state FEL for distances on the order of kilometers. The diffusion of particles in phase space has been evaluated numerically and can be adequately calculated by a simple linear model.

The important conclusion of this work is that by properly designing a TBA, one can minimize particle diffusion in phase space. In other words a TBA can be designed so that there is negligible loss of particles for practical lengths.

Acknowledgments

The authors would like to thank J. Wurtele and R. Marx for useful conversations and communications.

This work was supported by the Division of High Energy Physics, U.S. Department of Energy, under Contract No. DE-AC03-76SF00098.

References

1. A. M. Sessler in Laser Acceleration of Particles, AIP Conference Proceedings, 91, p. 151 (1982); D. B. Hopkins, A. M. Sessler and J. S. Wurtele, Nuclear Instruments and Methods in Physics Research, 228, 15 (1984).

2. J. S. Wurtele, "On Acceleration by the Transfer of Energy Between Two Beams," Laser Acceleration of Particles: II, AIP Conference Proceedings, ___, (1985) (to be published).

3. M. N. Kroll, P. L. Morton, M. N. Rosenbluth, "Free-Electron Lasers with Variable Parameter Wigglers," IEEE Journal of Quantum Electronics, QE-17 1436, (1981).

4. J. Guckenheimer, P. Holmes, Nonlinear Oscillations, Dynamical Systems, and Bifurcations of Vector Fields, Springer-Verlag p. 22-27, (1983).

5. F. Reif, Fundamentals of Statistical and Thermal Physics, McGraw-Hill, Chapter 15, (1965).

6. R. Marx, Lawrence Berkeley Laboratory Internal Note TBA-# (Aug. 1985), (unpublished); private communication.

Figure Captions

Figure 1. Schematic of a Two-Beam Accelerator.

Figure 2. The taper design is plotted for the first few sections of a TBA. The beam is bunched in a previous section and is injected on the left with $\gamma = 42$. The discontinuous jumps occur at the induction units. Fig. 2a shows γ_r and Fig. 2b shows a_w.

Figure 3. These are snapshots (Fig. 3a, 3b, 3c, 3d) of the phase space distribution of the electrons at various stages in a wiggler module. A distance was chosen far enough along the TBA to show that the system had reached a "steady-state." Between (c) and (d) the electrons are accelerated by an induction unit and injected into the next wiggler module.

Figure 4. This shows the actual phase space trajectory of an electron in a TBA. The trajectory begins at the top of the picture. The dashed vertical lines indicate when the electron passes through an induction unit. The numbers indicate the order of the jumps.

Figure 5. This is a Poincaré plot for three different electrons. The surface of section is taken immediately after the induction units. This is from a complete TBA simulation.

Figure 6. This shows Poincaré plots for ten different electrons at various distances from the closed trajectory. In (a) the electric field a_s is constant. In (b) and (c) a sin wave perturbation is superimposed on a_s. In (b) the frequency of the perturbation is far from resonance and the amplitude of the perturbation is 10% of a_s. In (c) the frequency of the perturbation is at resonance and the amplitude is 1% of a_s. Note that in (b) the surfaces are not broken up even though they are shifted. In (c) the surfaces are only disrupted near the center. This is because

non-linearities cause the surfaces further from the center to have lower frequencies.

Figure 7. This is a sample of the electric field from a complete TBA run.

Figure 8. This is the correlation function for a_s calculated in dimensionless units. (See Equation (12)).

Figure 9. This is the Fourier transform of the correlation function shown in Fig. 8. In these dimensionless units the oscillator frequency corresponds to $\Omega = 1.0$. The small peak at the right is a perturbation due to the induction units. Note that aside from this peak all the spectrum is below the linear oscillator frequency. This spectrum should be directly proportional to the power spectrum of the electric field.

Figure 10. This is a plot of the diffusion coefficient D vs the oscillation amplitude of the particle. This plot was arrived at by noting that the oscillation frequency changes with amplitude. Calculation based on equations (12) and (13).

Figure 11. In this plot, the induction units give a $\Delta\gamma = 5$ when one actually needs $\Delta\gamma = 4$ to match correctly between sections. As can be seen, this large mismatch is insufficient to destroy the closed surfaces in phase space.

Figure 12. This shows the diffusion coefficient for fluctuations in induction units. Here $\langle\delta\gamma^2\rangle = Dn$ where n is the number of induction units gone through. The error bars on the points represent the standard deviation of the statistical sample. The solid line is a least squares fit to the diffusion coefficients calculated from the simulation. The dashed line is the value of D predicted by the formula $D = \Delta\gamma_{max}^2/6$ from Eq. (18).

Table I. Design parameters for the steady-state section of the TBA.

Wiggler module length	= 200 cm	
γ_r, start of a period	= 42	which is 21.46 MeV
γ_r, end of a period	= 38	which is 19.42 MeV
Induction unit $\Delta\gamma$	= 4	which is 2.04 MeV
Magnetic field a_w, start of period	= 5.265	which is 2.954 kG peak field
Magnetic field a_w, end of period	= 4.775	which is 2.679 kG peak field
ψ_r	= 0.0967	
Wiggler period	= 27 cm	
Radiation wavelength	= 1.0 cm	
Electric field a_s	= 0.2548	which is 1.193×10^8 volts/m peak field
Loss parameter α	= 0.1127	
Current	= 2400 amps	
Bunching parameter $\langle\cos\psi\rangle$	= 0.75	
Waveguide size	= 5 x 2 cm	
Mode used	= TE_{01}	

Table II. Values of the diffusion coefficient D as measured in the computer simulation. The value was measured for several different values of the oscillation amplitude. The error estimate is given by $\sigma_D/\sqrt{n}$ where σ_D is the standard deviation of the sample measurements and n is the number of samples.

$\delta\gamma_{max}$	$D \times 10^{-3}$	Error estimate for $D \times 10^{-3}$
1.369	4.9	1.0
3.268	4.9	0.8
5.053	5.8	0.7
6.795	7.1	0.8
9.703	13.9	4.7

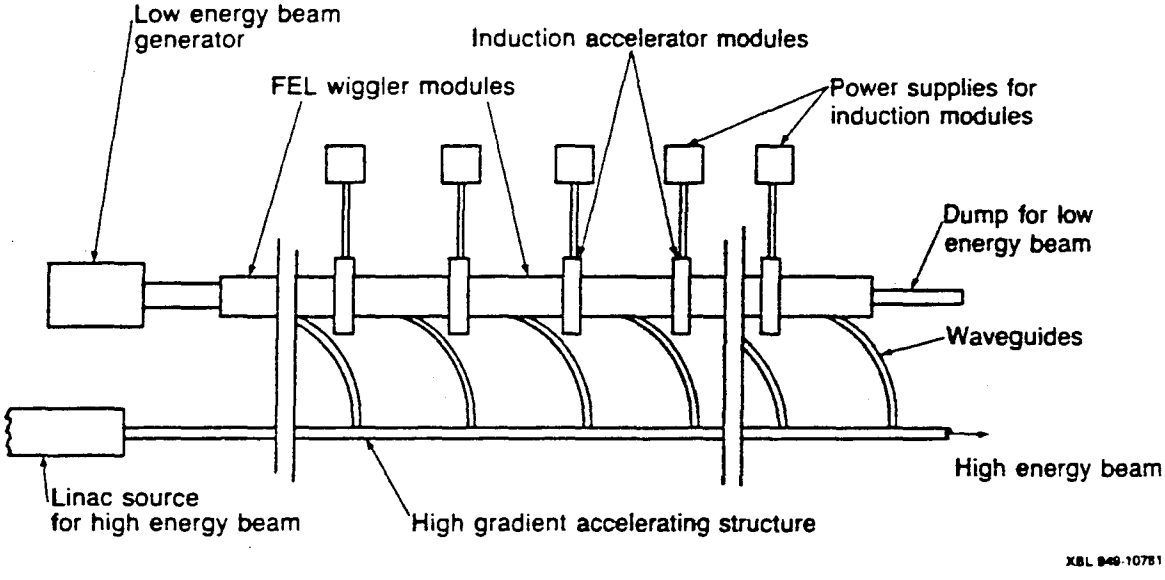
Low energy beam generator
Induction accelerator modules
FEL wiggler modules
Power supplies for induction modules
Dump for low energy beam
Waveguides
High energy beam
Linac source for high energy beam
High gradient accelerating structure
XBL 849-10781

Figure 1

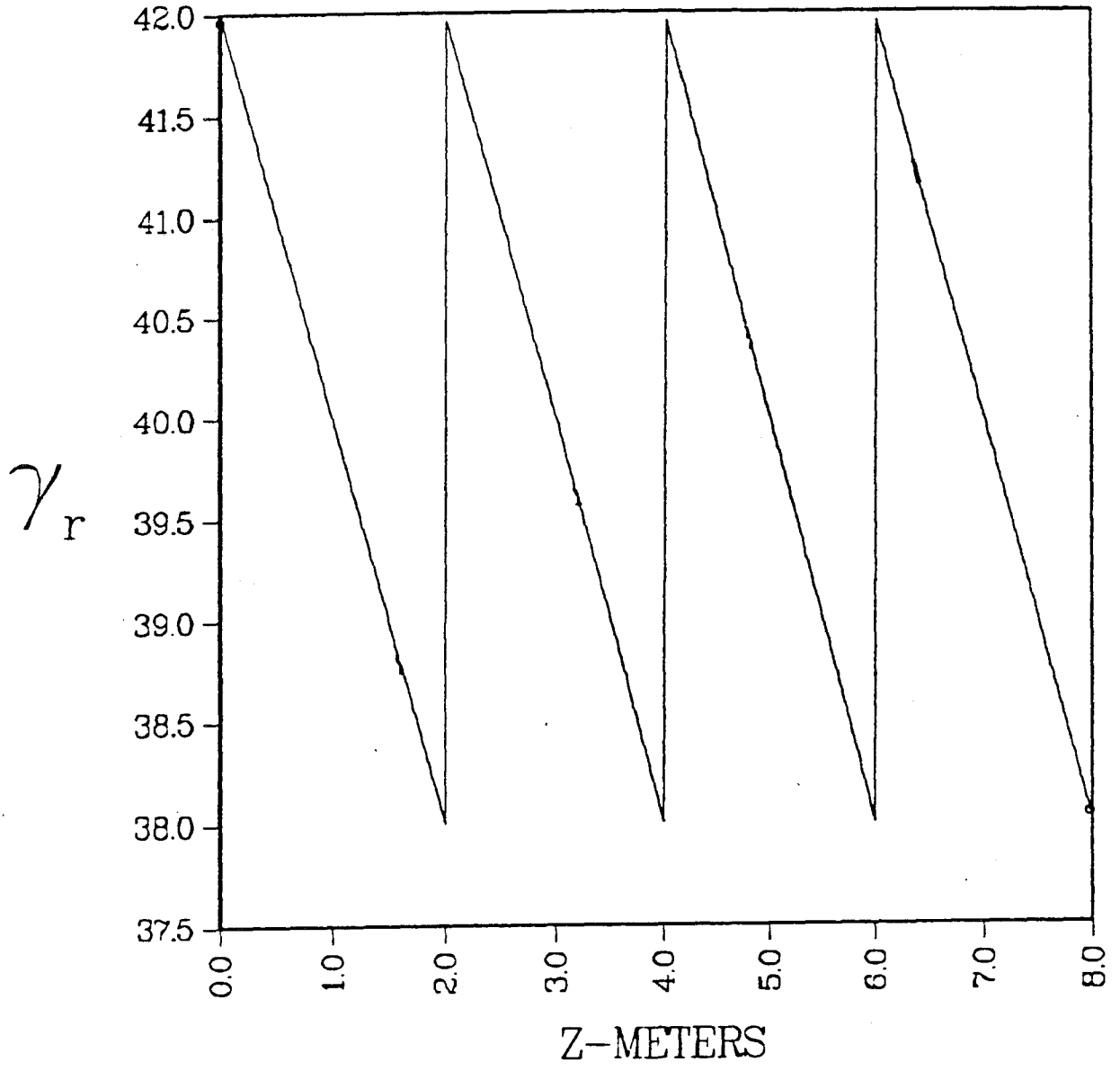

XBL 858-3527

Figure 2a

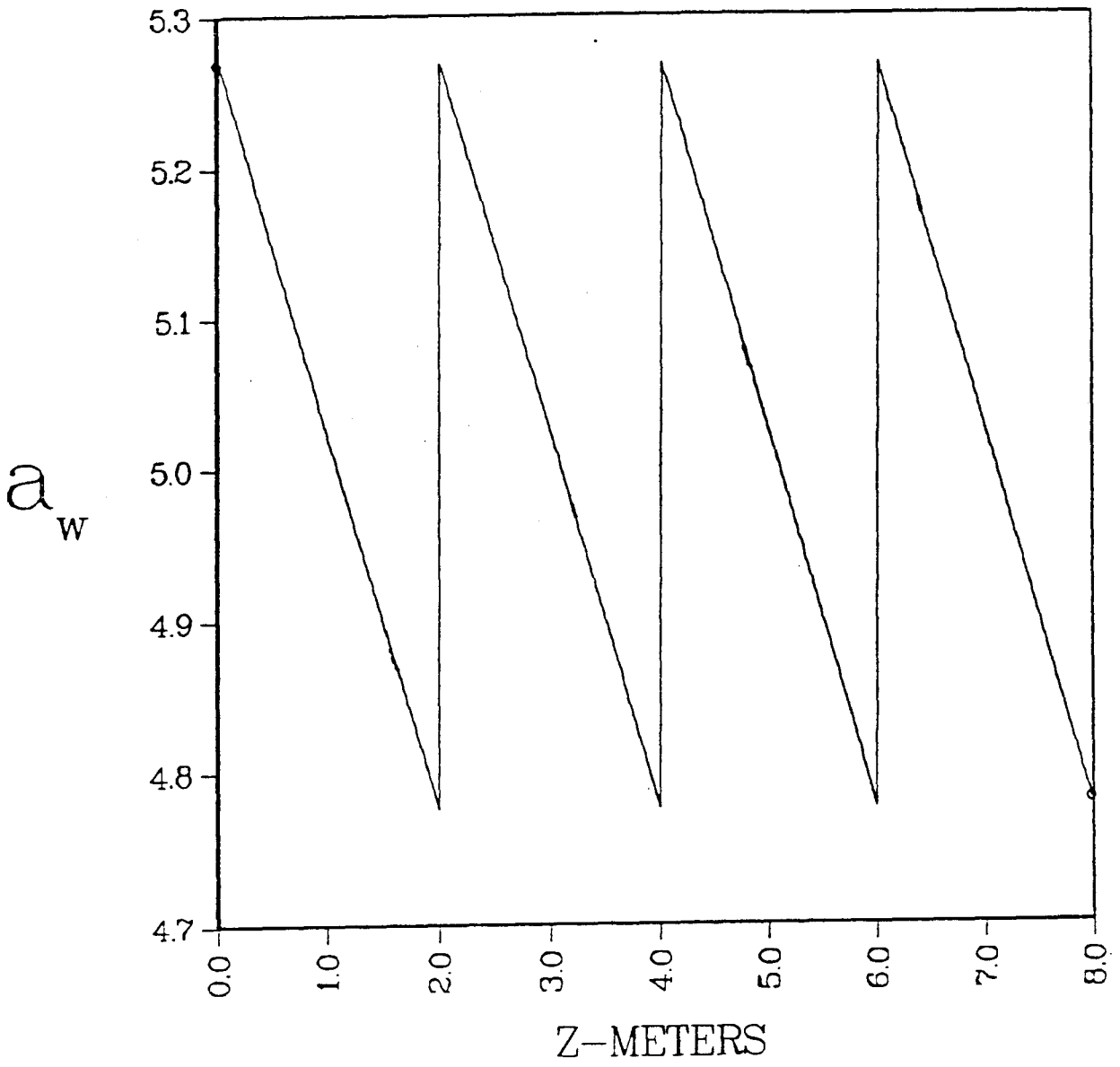

XBL 858-3526

Figure 2b

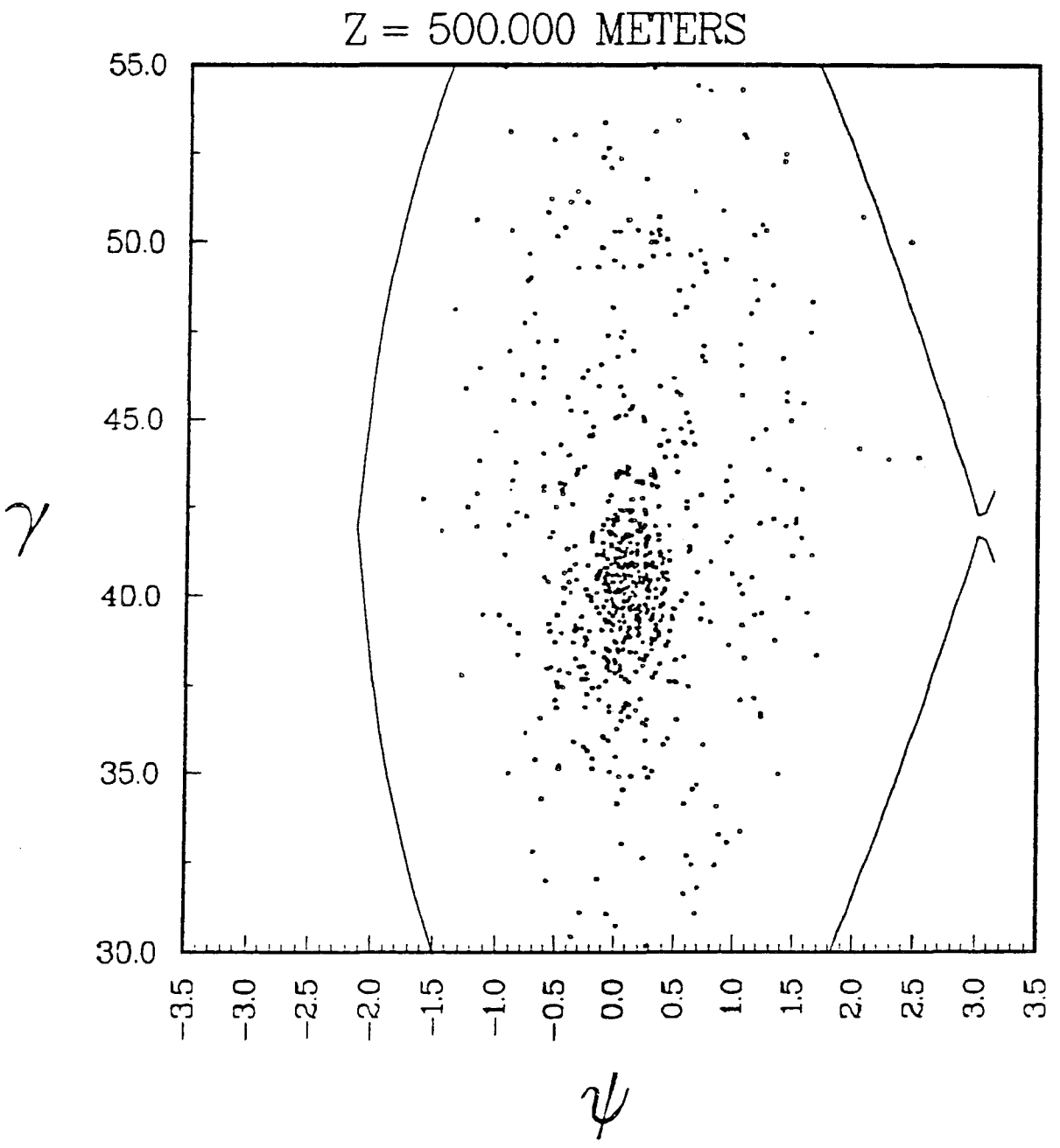

XBL 858-3525

Figure 3a

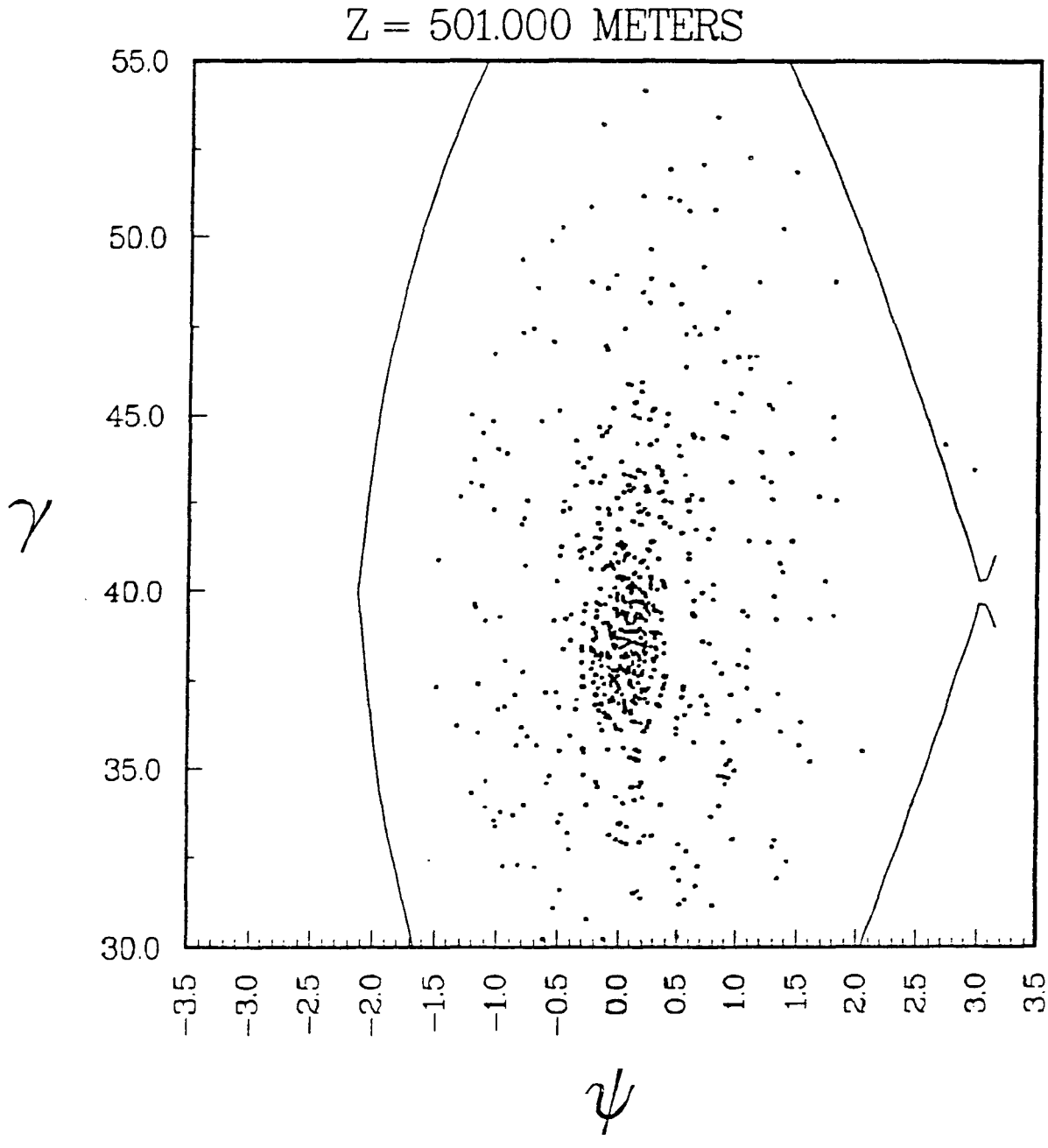

XBL 858-3524

Figure 3b

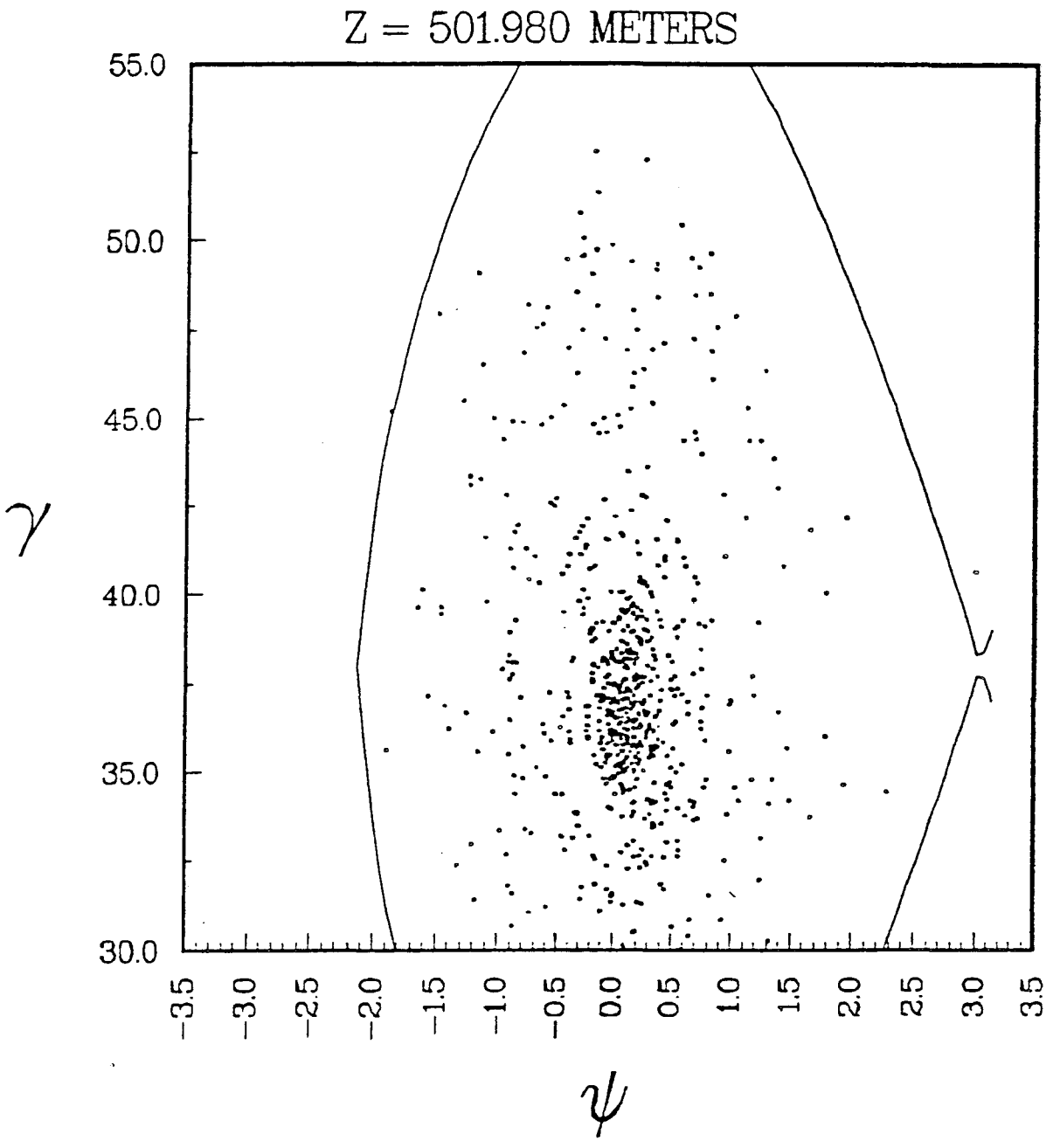

XBL 858-3523

Figure 3c

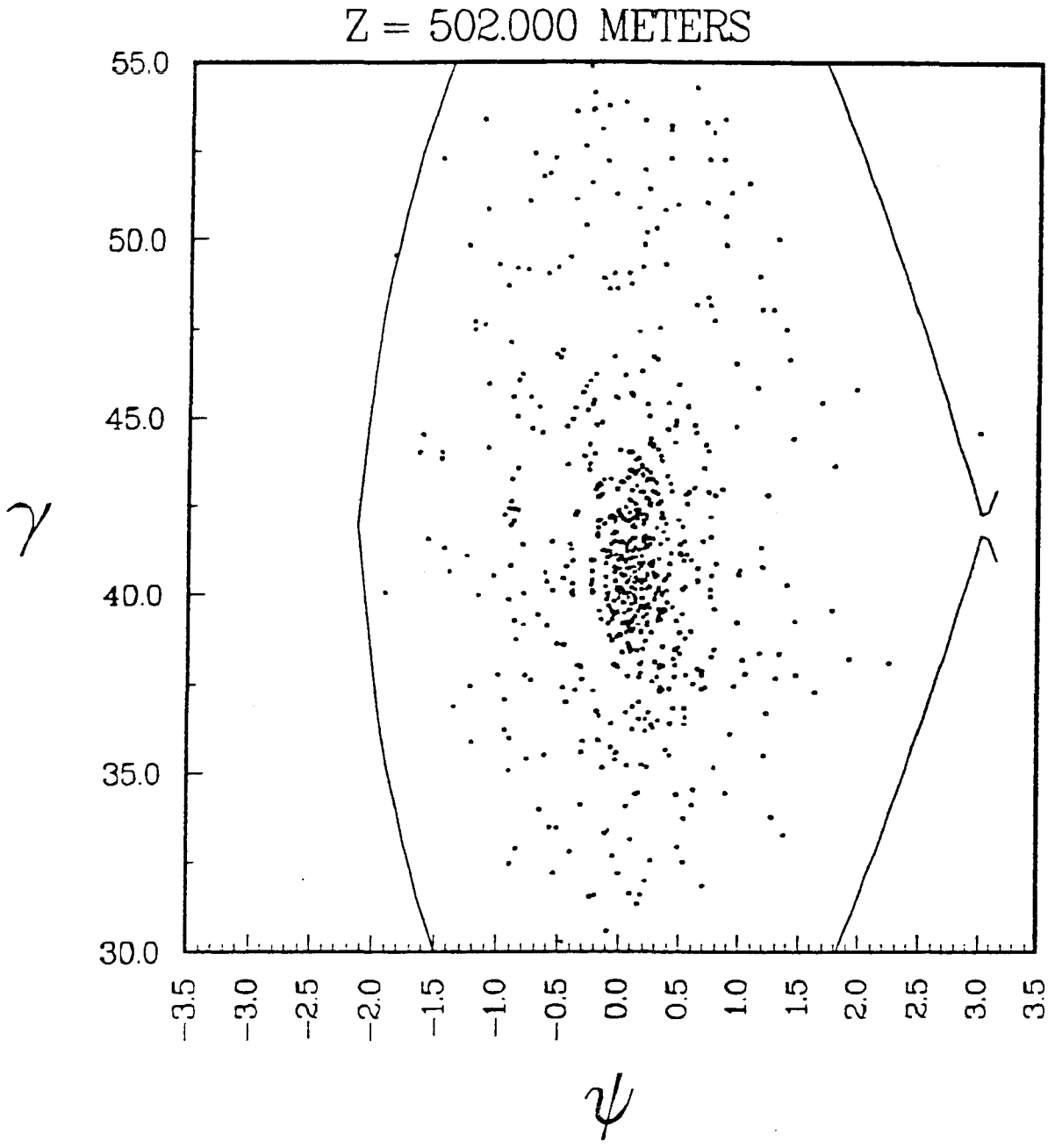

XBL 858-3522

Figure 3d

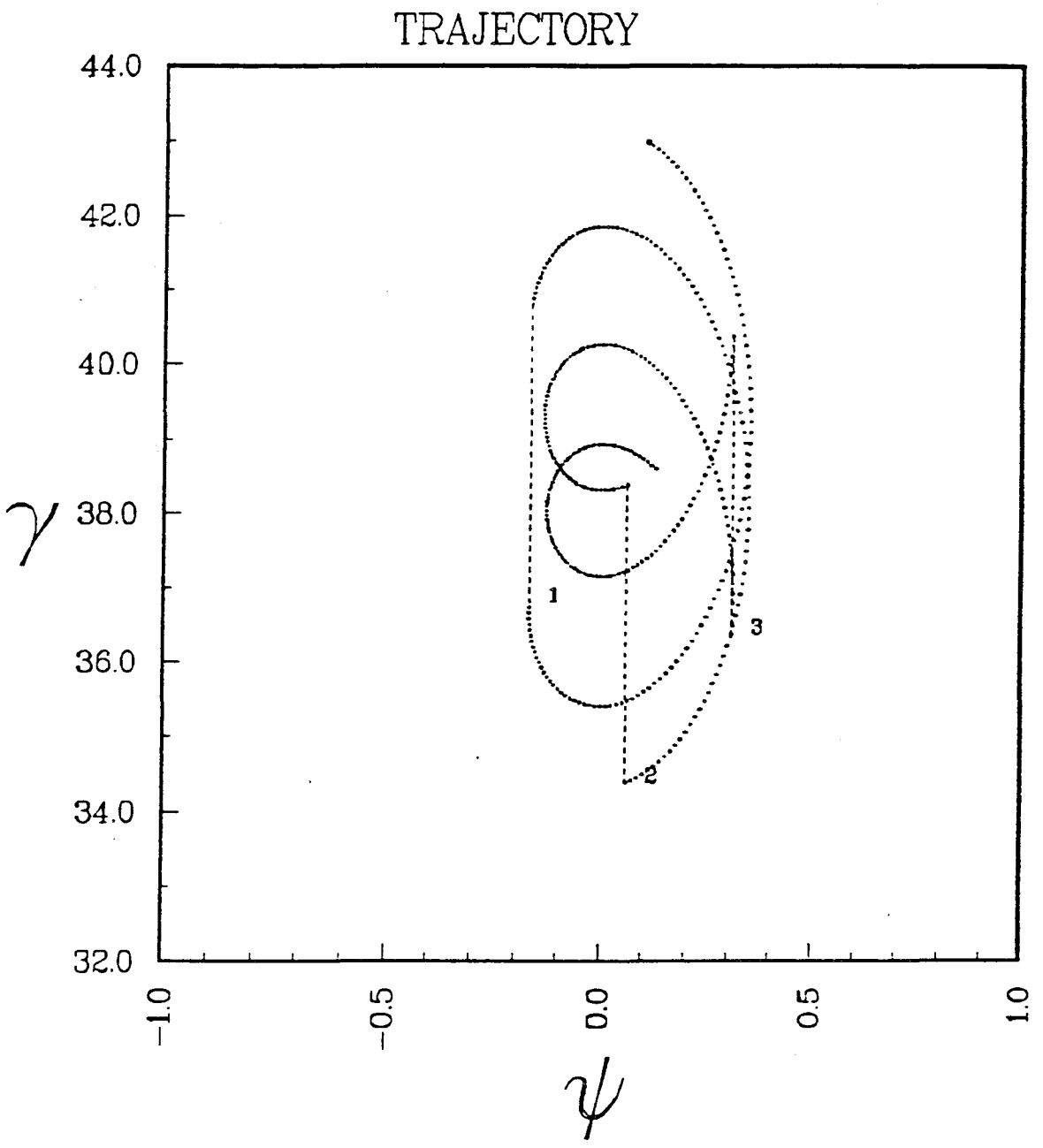

XBL 858-3521

Figure 4

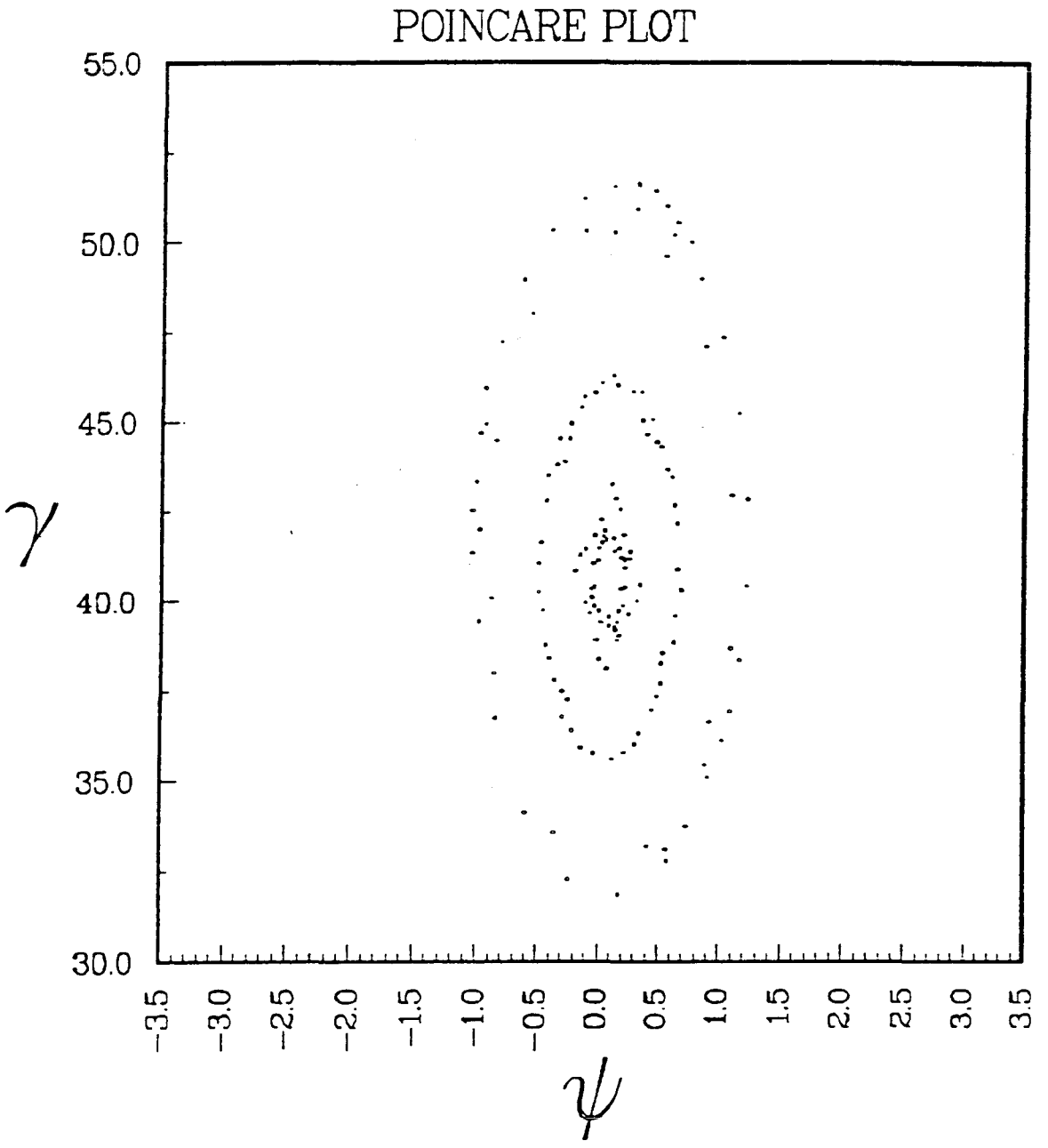

XBL 858-3520

Figure 5

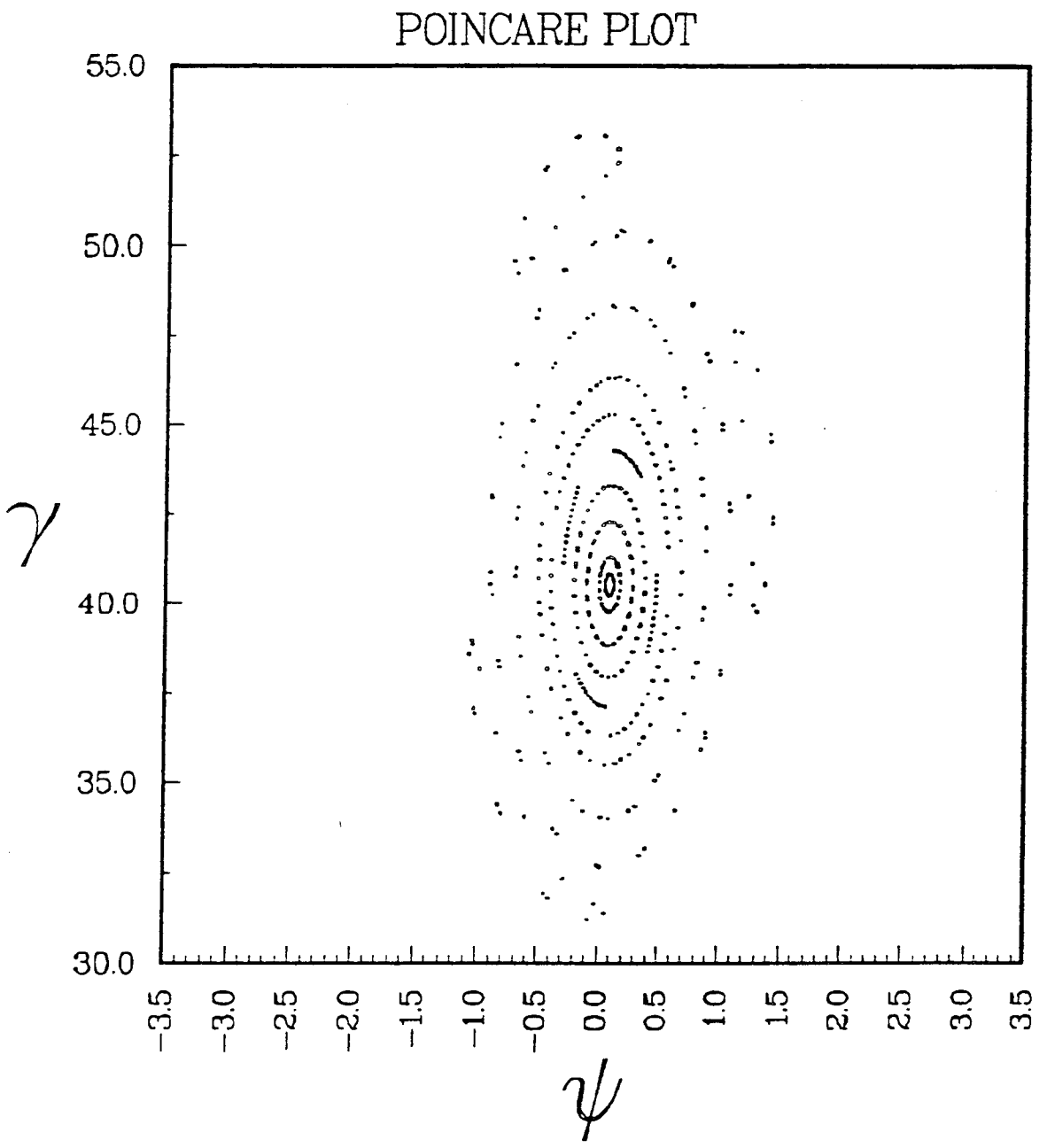

XBL 858-3519

Figure 6a

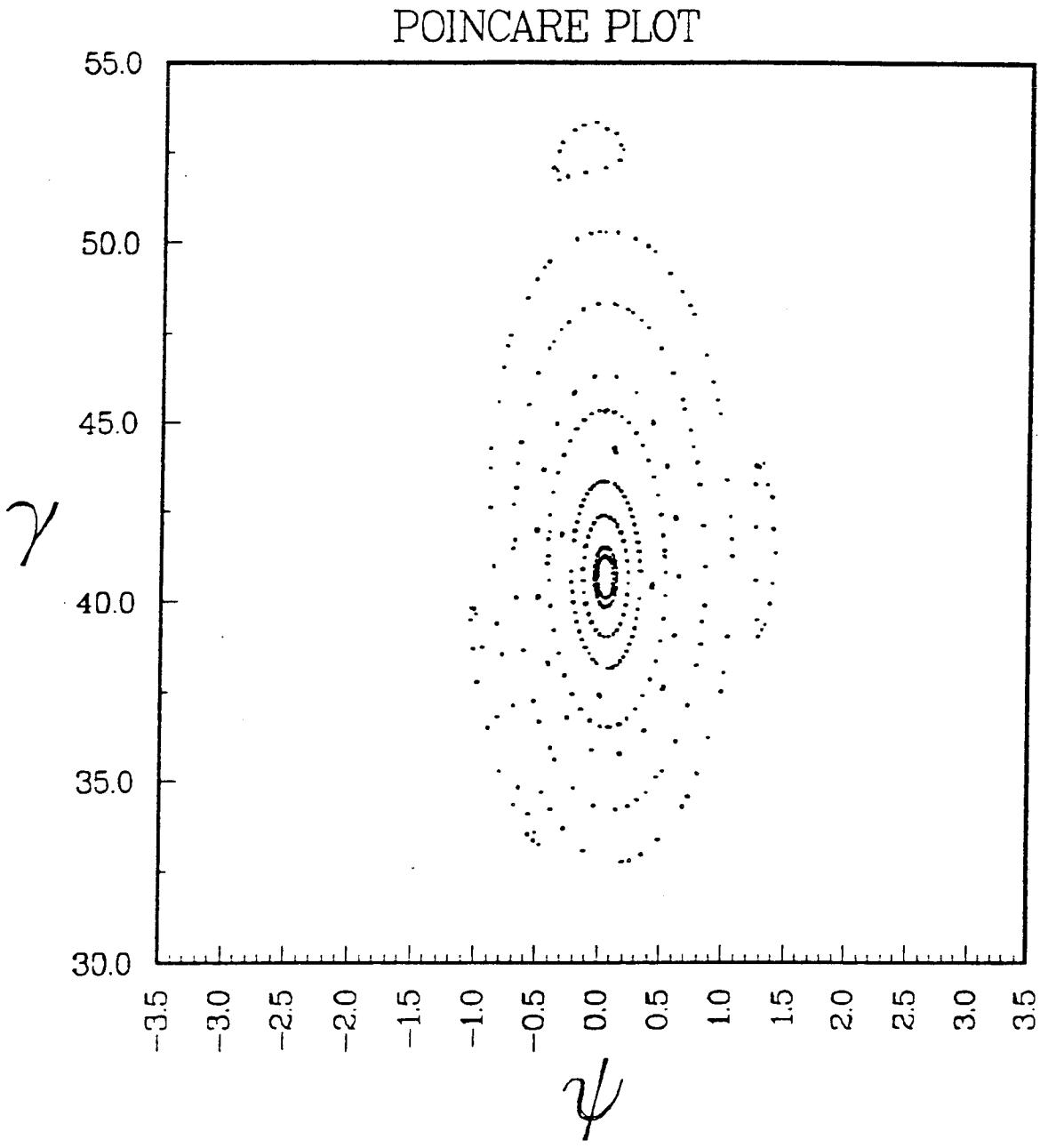

XBL 858-3518

Figure 6b

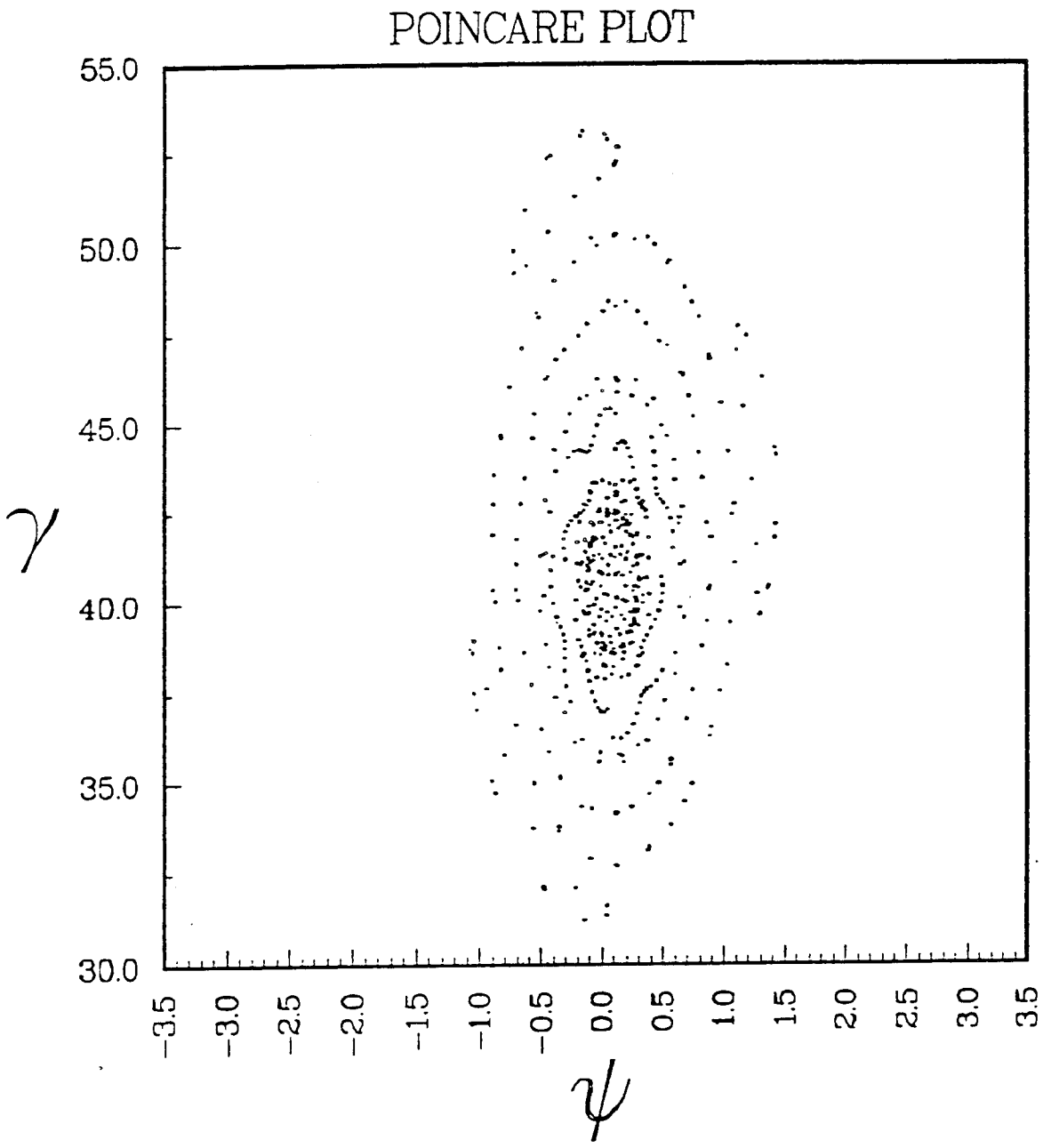

XBL 858-3517

Figure 6c

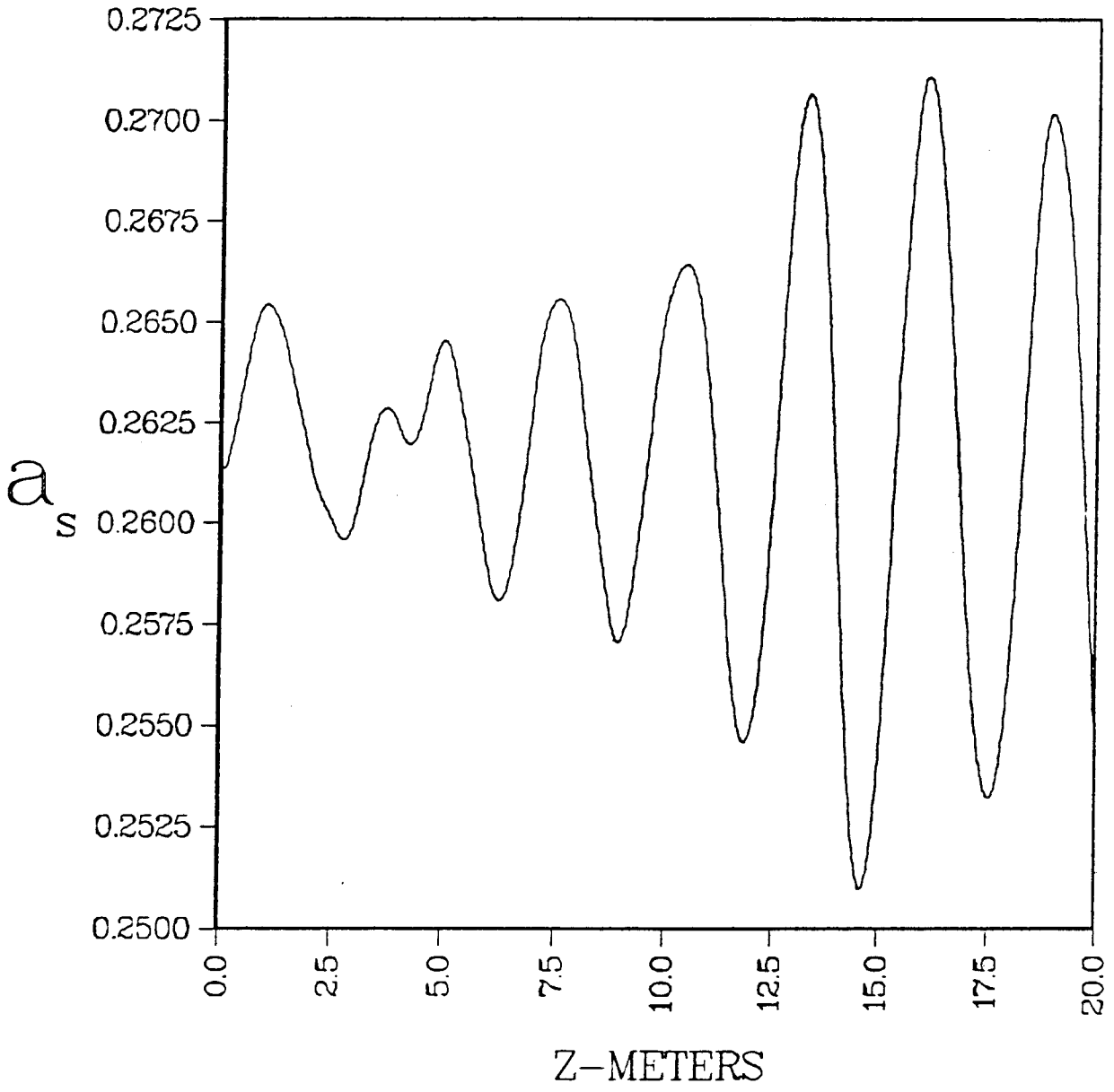

XBL 858-3515

Figure 7

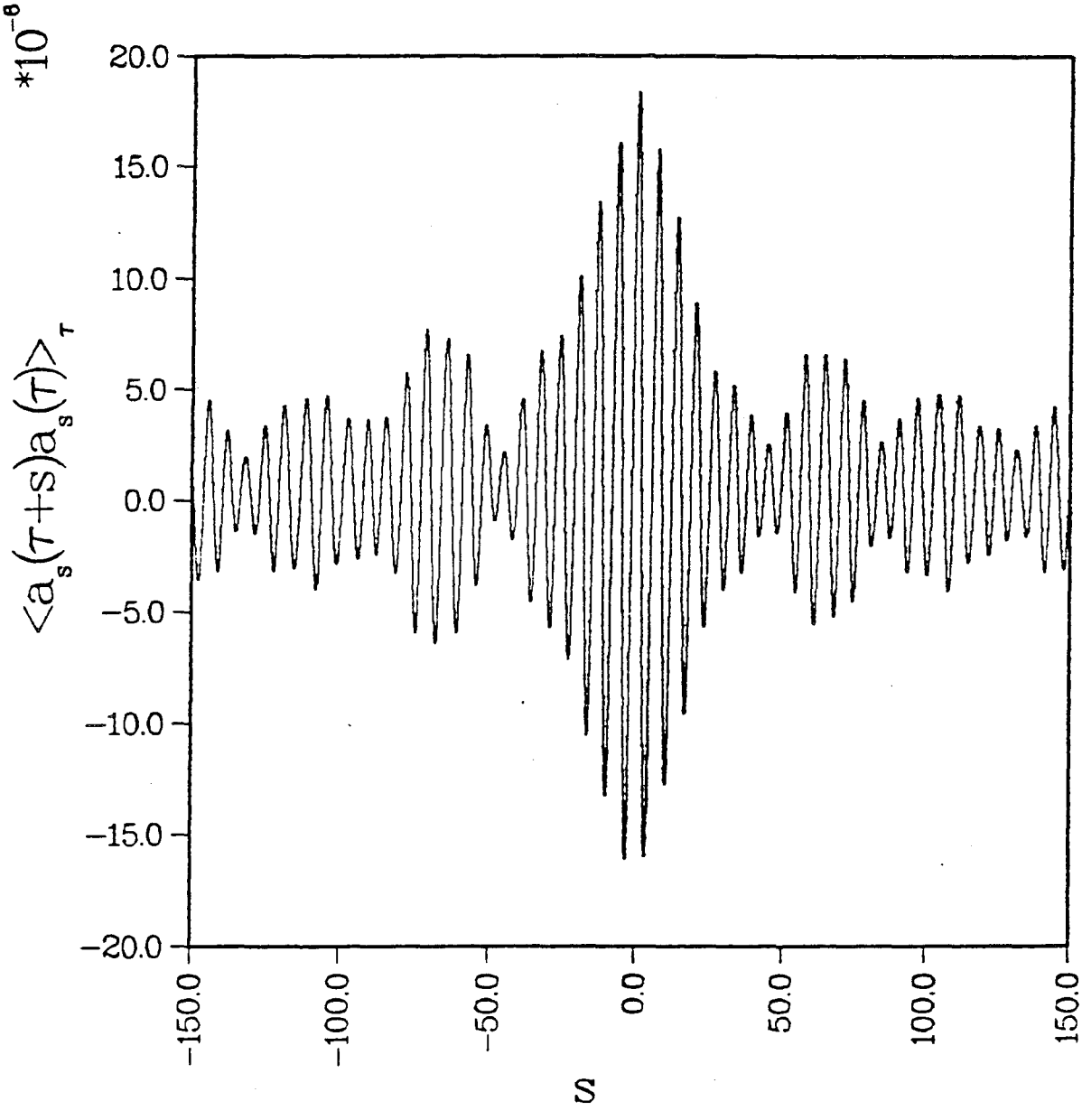

XBL 858-3516

Figure 8

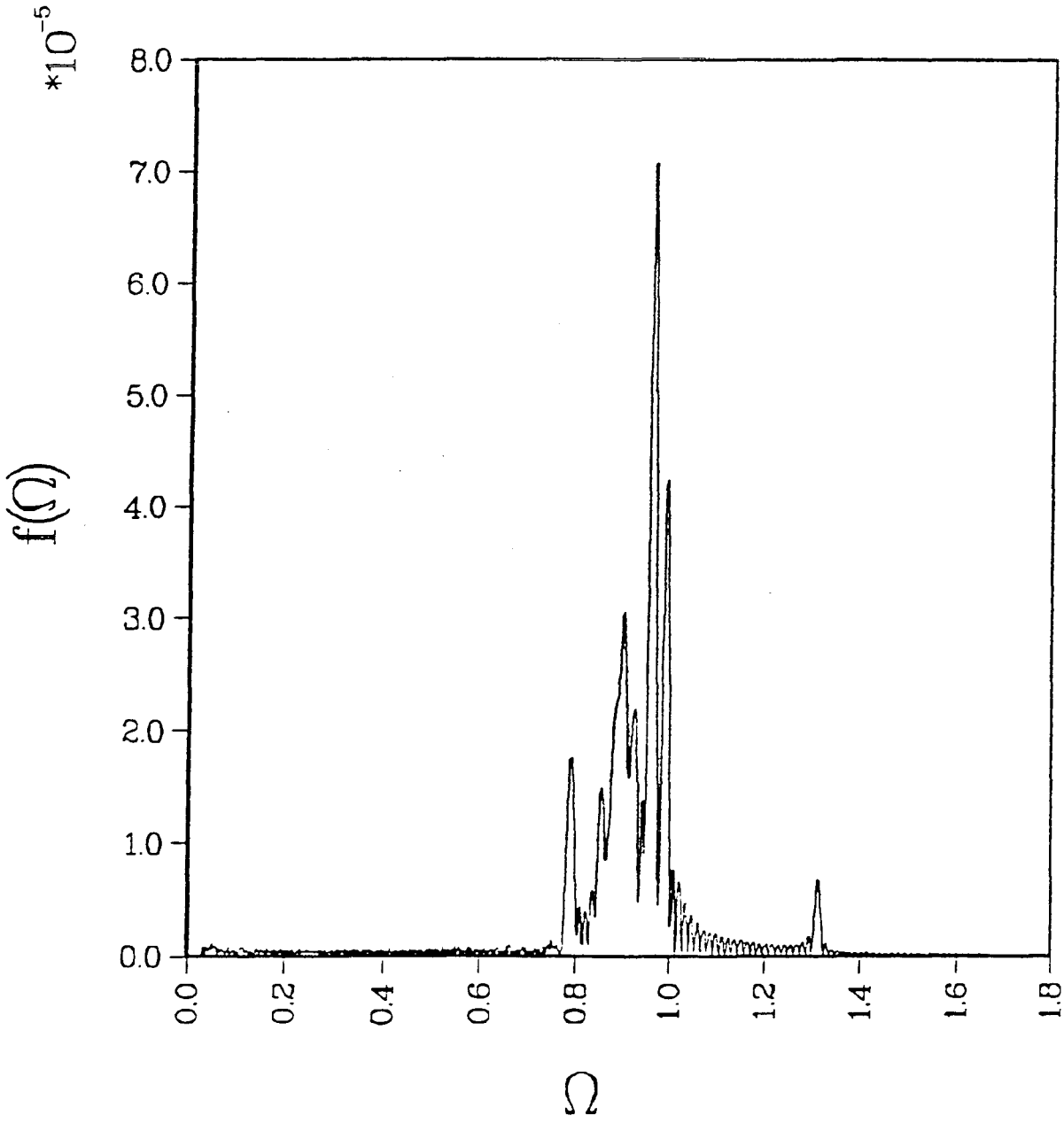

XBL 858-3514

Figure 9

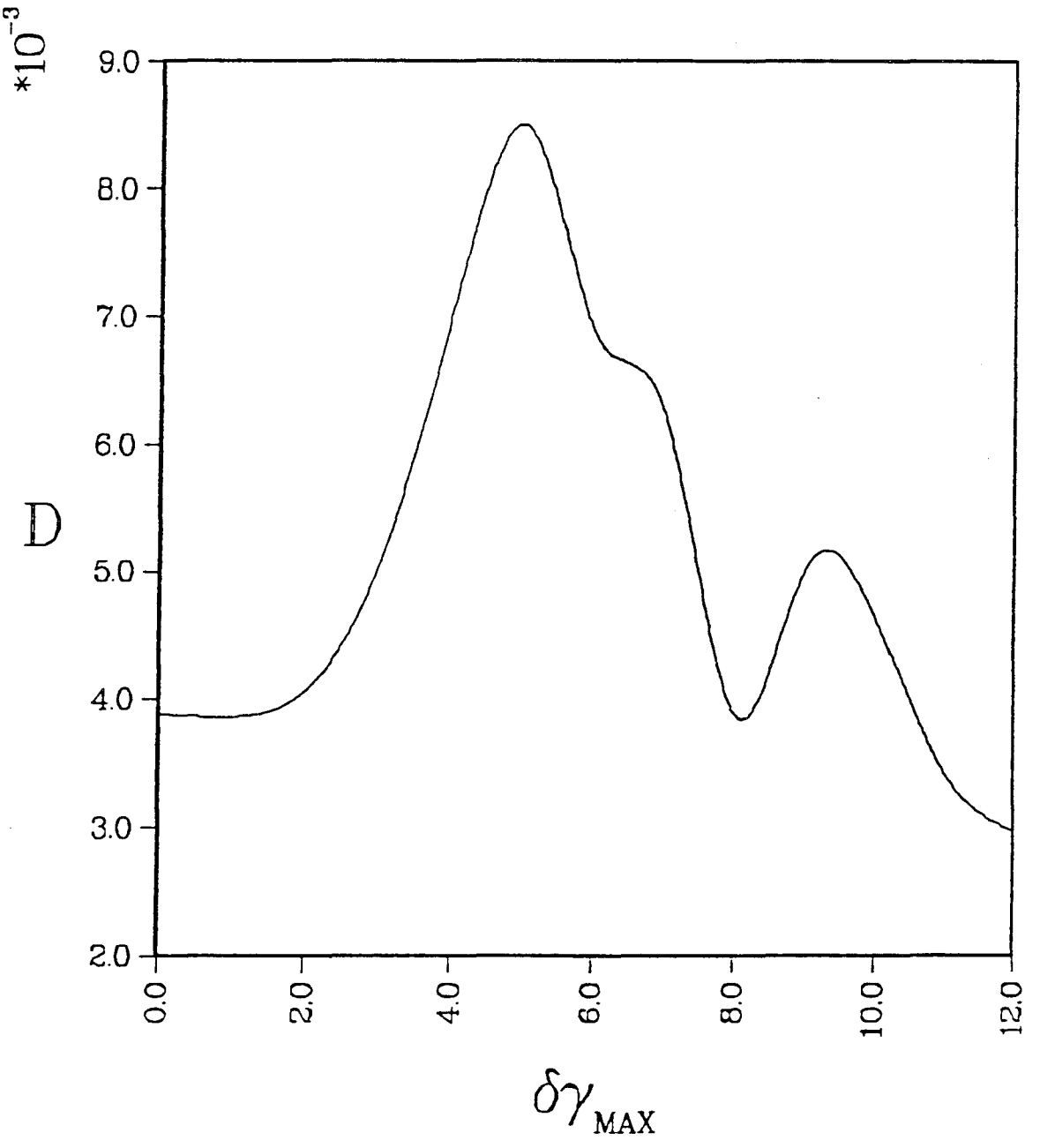

XBL 858-3512

Figure 10

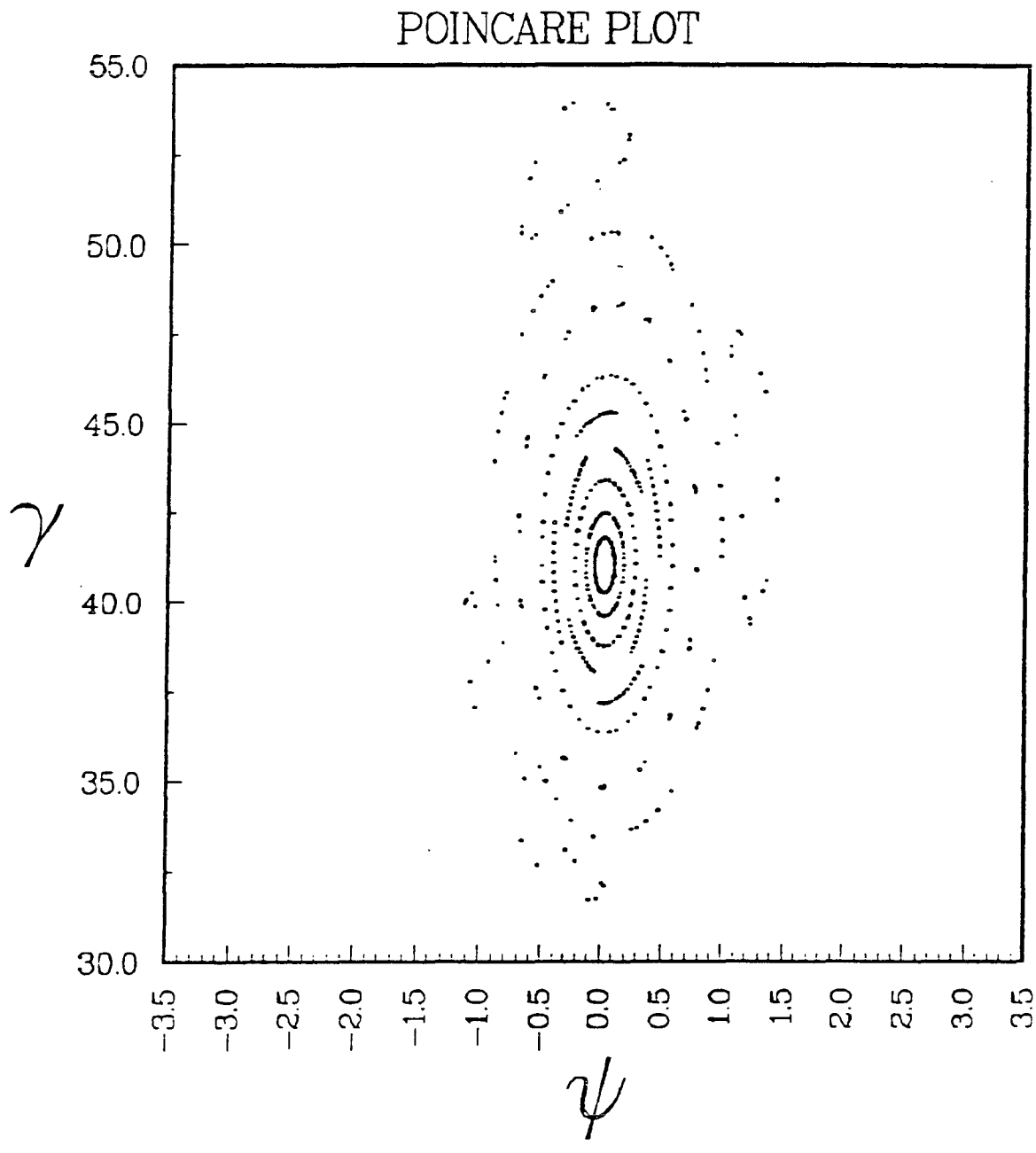

XBL 858-3513

Figure 11

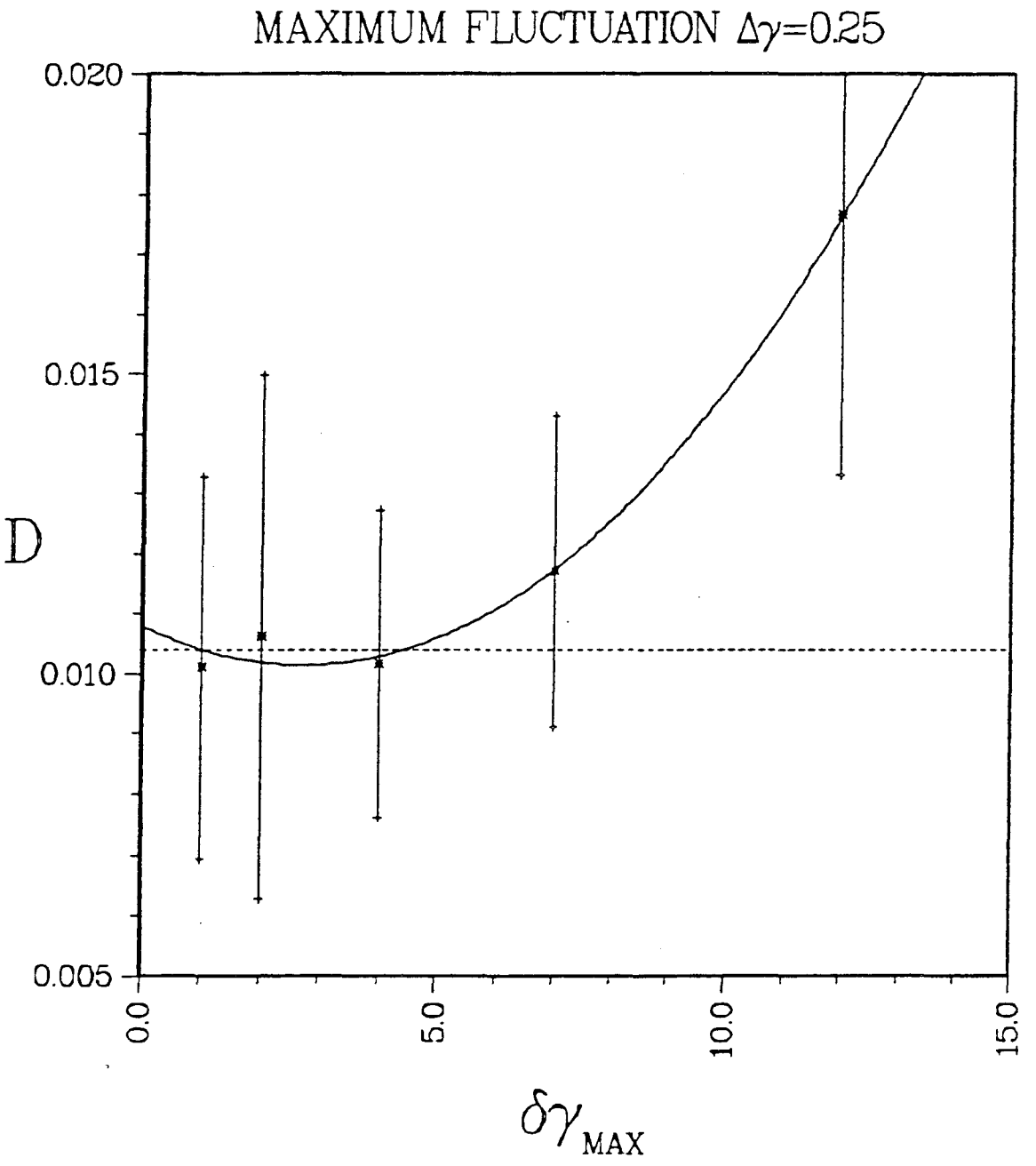

XBL 858-3511

Figure 12